

# Catadioptric Camera Calibration Using Geometric Invariants\*

Xianghua Ying, Zhanyi Hu

National Laboratory of Pattern Recognition, Institute of Automation  
Chinese Academy of Sciences, 100080 P.R.China  
{xhying, huzy} @nlpr.ia.ac.cn

## Abstract

*Central catadioptric cameras are imaging devices that use mirrors to enhance the field of view while preserving a single effective viewpoint. In this paper, we propose a novel method for the calibration of central catadioptric cameras using geometric invariants. Lines in space are projected into conics in the catadioptric image plane as well as spheres in space. We proved that the projection of a line can provide three invariants whereas the projection of a sphere can provide two. From these invariants, constraint equations for the intrinsic parameters of catadioptric camera are derived. Therefore, there are two variants of this novel method. The first one uses the projections of lines and the second one uses the projections of spheres. In general, the projections of two lines or three spheres are sufficient to achieve the catadioptric camera calibration. One important observation in this paper is that the method based on the projections of spheres is more robust and has higher accuracy than that using the projections of lines. The performances of our method are demonstrated by the results of simulations and experiments with real images.*

## 1. Introduction

In many computer vision applications, including robot navigation, virtual reality, and image-based rendering, a camera with a quite large field of view is required. The conventional camera has a very limited field of view. One effective way to enhance the field of view of a camera is to combine the camera with mirrors. There are some representative implementations of catadioptric imaging systems described in [3] and [11~14]. Recently, Baker and Nayar [1] investigate these catadioptric systems with respect to a single viewpoint constraint. Catadioptric systems can be classified into two classes, central and noncentral, depending on whether they keep single viewpoint or not. This paper aims at the calibration of central catadioptric cameras.

---

\*This work was supported by the National Natural Science Foundation China under grant No. 6003301, and the National Key Basic Research and Development Program China (973) under grant No. 2002CB312104.

Here is a brief review of the methods used by other researchers for the central catadioptric camera calibration.

### 1. Known world coordinates

This kind of methods uses a calibration pattern with control points whose 3D world coordinates are known. These control points can be corners, dots, or any features that can be easily extracted from the images. Using iterative methods extrinsic parameters (position and orientation) and intrinsic parameters can be recovered [4].

### 2. Self-calibration

This kind of calibration techniques uses only point correspondences in multiple views, without needing to know either the 3D location of the points or the camera locations. But it is well known that determining stereo correspondences is a difficult issue in computer vision. Kang [5] uses the consistency of pairwise tracked point features across a sequence to develop a reliable calibration method for a para-catadioptric camera.

### 3. Projections of lines

This kind of methods uses only the images of lines in the scene, without needing to know any metric information. Geyer and Daniilidis [7] use images of two sets of parallel lines to find the intrinsic parameters as well as the orientation of the plane containing the two parallel line sets. Barreto and Araújo [6] present a two-step method: firstly, the principal point is determined using the intersections of three catadioptric line images. Secondly, the recovered principal point is used to determine the image of the absolute conic from these line images and the intrinsic parameters are recovered by means of Cholesky factorization. More recently, Geyer and Daniilidis [8] propose another calibration method for a para-catadioptric camera using the projective properties of the images of three lines.

In this paper, we propose a novel calibration method based on the geometric invariants, which provides a unified framework for the calibration using either images of lines or images of spheres. The motivations for proposing this novel method are based on the following facts:

1) Lines and spheres are all common geometric entities in real scenes, and they are often used for the conventional camera calibration. It is well known that, under central catadioptric cameras, a line in space is projected into a conic in the image plane [2][3]. We

further prove that the occluding contour of a sphere in space is also a conic in the catadioptric image plane. Based on this fact, we present a unified framework to cover both the projections of lines and those of spheres.

2) Using the unified framework, we proved that, in general, the projection of a space line can provide three invariants whereas the projection of a space sphere can provide two, without needing to know the 3D locations of the line and the sphere. From these invariants, the constraint equations for the intrinsic parameters can be derived. Therefore, the projections of either two lines or three spheres are sufficient to achieve the catadioptric camera calibration (note that Geyer and Daniilidis [9] only discuss the number of constraints provided by a line image, but no actual constraint equations are given). Different from the methods proposed in [6] and [7] which must use the intersections of line images to determine the principle point at the first step, our method directly uses the constraint equations provided by single-line or single-sphere image. One advantage of our method is that we can perform the calibration in the case where the minimum number of line or sphere images is available. Another advantage of our method is that in the case where the number of line or sphere images is not sufficient for full intrinsic parameter calibration (e.g., only one line image is available), the calibration can also be done partially using our method if we assume that some intrinsic parameters are known in advance. We further realize that the method proposed in [8] is a special case within our general treatment of the topic.

3) One important contribution of this paper is to introduce spheres for the central catadioptric camera calibration. Although lines and spheres are all projected into conics in the image plane, it is more difficult to extract the projection of a line with high accuracy than that of a sphere. The main reason for this is, the projection of a line (usually a line segment in real scene) is only a portion of a conic (e.g. about one-third of an ellipse) but the projection of a sphere is usually a closed ellipse, and conic fitting using points lying on a portion of a conic is an error-prone process. As we know, the accuracy of the estimated intrinsic parameters highly depends on the accuracy of the extracted conics. Therefore, sphere images are preferred in the case where accurate calibration of central catadioptric cameras is needed.

## 2. A generalized image formation model for central catadioptric cameras

Baker and Nayar [1] show that the only useful physically realizable mirror surfaces of catadioptric cameras that produce a single viewpoint are planar, ellipsoidal, hyperboloidal, and paraboloidal. Recently,

Geyer and Daniilidis [9] propose a generalized image formation model for these central catadioptric cameras. They prove that the central catadioptric image formation is equivalent to a two-step mapping via a sphere:

**Step 1:** A point in the 3D space is projected to a unit sphere centered at the single effective viewpoint.

The unit sphere is called the viewing sphere. Considering a general 3D space point, visible by a catadioptric camera, with Cartesian coordinates  $X = (x_w \ y_w \ z_w)^T$  in the world coordinate system whose origin is at the single viewpoint, the projection of  $X$  on the viewing sphere is:

$$X_s = (x_s \ y_s \ z_s)^T = \left( \frac{x_w}{\sqrt{x_w^2 + y_w^2 + z_w^2}} \quad \frac{y_w}{\sqrt{x_w^2 + y_w^2 + z_w^2}} \quad \frac{z_w}{\sqrt{x_w^2 + y_w^2 + z_w^2}} \right)^T. \quad (1)$$

**Step 2:** The point  $X_s$  on the viewing sphere is perspectively projected to  $m$  on the image plane  $\Pi$  from another point  $O_c$ . The image plane  $\Pi$  is perpendicular to the line determined by the single viewpoint  $O$  and  $O_c$  (see Figure 1).

This step can be considered as taking image of the viewing sphere using a virtual camera whose optical center is located at  $O_c$  and whose optical axis coincides with the line determined by  $O$  and  $O_c$ . Once the intrinsic parameters of the virtual camera are estimated, the intrinsic parameters of the central catadioptric camera are known. In general, we distinguish 5 intrinsic parameters for the virtual camera: the principal point  $O_p (u_0, v_0)$ , the effective focal length  $f_e = |O_c O_p|$ , the aspect ratio  $r$  and the skew factor  $s$ . The intrinsic matrix is written as:

$$K = \begin{bmatrix} r \cdot f_e & s & u_0 \\ & f_e & v_0 \\ & & 1 \end{bmatrix}. \quad (2)$$

The distance,  $l = |OO_c|$ , can be regarded as another parameter of the catadioptric camera. Therefore, there are totally six parameters required to be calibrated. The projection of  $X_s$ , i.e.,  $m = (x \ y \ 1)^T$  on the catadioptric image plane  $\Pi$ , satisfies:

$$\lambda m = K [R \ t] \begin{bmatrix} x_s \\ y_s \\ z_s \\ 1 \end{bmatrix} = K \begin{bmatrix} 1 & & & \\ & 1 & & \\ & & 1 & \\ & & & l \end{bmatrix} \begin{bmatrix} x_s \\ y_s \\ z_s \\ 1 \end{bmatrix}, \quad (3)$$

where  $\lambda$  is an unknown scale factor.

For the revolution conic section mirror, it satisfies:

$$l = \frac{2\varepsilon}{1 + \varepsilon^2}, \quad (4)$$

where  $\varepsilon$  is the eccentricity of the conic. The relationship between eccentricity  $\varepsilon$  and distance  $l$  for different types of central catadioptric cameras is shown in Table 1.

	Ellipsoidal	Paraboloidal	Hyperboloidal	Planar
$\varepsilon$	$0 < \varepsilon < 1$	$\varepsilon = 1$	$\varepsilon > 1$	$\varepsilon \rightarrow \infty$
$l$	$0 < l < 1$	$l = 1$	$0 < l < 1$	$l = 0$

**Table 1:** Eccentricity  $\varepsilon$  and distance  $l$

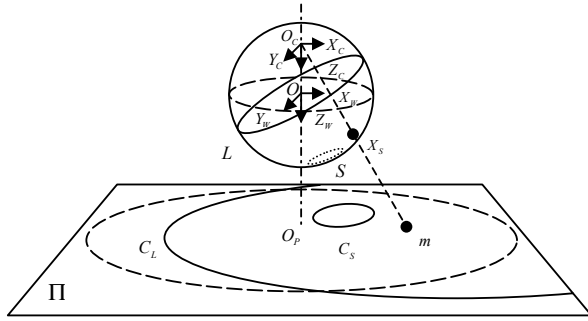


**Figure 1:** The generalized image formations of a point (as illustrated in Section 2), a line, and a sphere (as illustrated in Section 3) in space are shown respectively. A space point is projected to point  $X_S$  on the viewing sphere, which then projected to  $m$  on the image plane  $\Pi$  from  $O_C$ . A sphere in space is projected to a small circle  $S$  on the viewing sphere, which then projected to a conic section  $C_S$  on the image plane from  $O_C$ . A line in space is projected to a great circle  $L$  on the viewing sphere, which then projected to a conic section  $C_L$  on the image plane. The equator is mapped to the dashed circle on the image plane.

### 3. Invariants of line and sphere images

In this section, firstly the equations of line and sphere images under the metric catadioptric projection are derived. Secondly, the invariants are obtained from the projection equations derived before. Finally, the constraint equations for the intrinsic parameters are derived from these invariants.

#### 3.1. Equations of line and sphere images

**Definition 1.** The metric catadioptric projection is a projection induced by a central catadioptric camera whose intrinsic parameters are as follows:  $r = 1$ ,  $s = 0$ ,  $u_0 = 0$ , and  $v_0 = 0$ . Correspondingly, the projection induced by a central catadioptric camera whose intrinsic parameters are defined by (2) is called the generic catadioptric projection.

For the case of the metric catadioptric projection, the camera intrinsic matrix can be rewritten as:

$$K_M = \begin{bmatrix} f_e & & & \\ & f_e & & \\ & & & 1 \end{bmatrix}. \quad (5)$$

Under the metric catadioptric projection, the origin of the image coordinate system is located at the principal point, and the geometric properties of the projections of lines and spheres can be easily discovered. These geometric properties will be described as invariants in Section 3.2.

The generalized image formations of a line and a sphere in space are shown in Figure 1. It is well known that a line in space is projected to a great circle whereas the occluding contour of a sphere in space is a small circle on the viewing sphere. A great circle is a circle defined by the intersection of the sphere and a plane passing through the spherical center, and a small circle is a circle on the sphere which is not a great circle. Assume a small circle, the occluding contour of a sphere on the viewing sphere, lies on a plane  $(n_x \ n_y \ n_z \ d_0)^T$ , where  $(n_x \ n_y \ n_z)^T$  is the unit normal vector for the plane, and  $d_0$  is the distance from the origin  $O$  to the plane, then a point  $(x_s \ y_s \ z_s)^T$  on the small circle satisfies:

$$\begin{cases} n_x x_s + n_y y_s + n_z z_s + d_0 = 0 \\ x_s^2 + y_s^2 + z_s^2 = 1 \end{cases}. \quad (6)$$

Similarly, a great circle, the image of a line on the viewing sphere, lies on a plane  $(n_x \ n_y \ n_z \ 0)^T$  passing through the origin  $O$ , then a point  $(x_s \ y_s \ z_s)^T$  on the great circle satisfies:

$$\begin{cases} n_x x_s + n_y y_s + n_z z_s = 0 \\ x_s^2 + y_s^2 + z_s^2 = 1 \end{cases}. \quad (7)$$

Obviously, a great circle can be considered as a special case of a small circle where the distance from the origin to the plane is zero (i.e., setting  $d_0 = 0$  in (6), we can obtain (7)). Therefore, there exists a unified framework to represent the projections of a line and a sphere on the viewing sphere. Consequently, the equations for a sphere derived from (6) can be changed into the equations for a line after setting  $d_0 = 0$ . Substituting (5) into (3), we get:

$$\lambda x = \lambda \begin{bmatrix} x \\ y \\ 1 \end{bmatrix} = \begin{bmatrix} f_e & & & \\ & f_e & & \\ & & & 1 \end{bmatrix} \begin{bmatrix} 1 & 0 \\ & 1 & 0 \\ & & 1 & l \end{bmatrix} \begin{bmatrix} x_s \\ y_s \\ z_s \\ 1 \end{bmatrix}. \quad (8)$$

Eliminate  $x_s, y_s, z_s$  and  $\lambda$  from (6) and (8), and rewrite in matrix form, then we obtain:

$$\begin{bmatrix} x \\ y \\ 1 \end{bmatrix}^T \begin{bmatrix} (l^2 - 1)n_x^2 + (d_0 + l \cdot n_z)^2 & (l^2 - 1)n_x n_y & (ld_0 + n_z)f_e n_x \\ (l^2 - 1)n_x n_y & (l^2 - 1)n_y^2 + (d_0 + l \cdot n_z)^2 & (ld_0 + n_z)f_e n_y \\ (ld_0 + n_z)f_e n_x & (ld_0 + n_z)f_e n_y & f_e^2 (d_0^2 - n_z^2) \end{bmatrix} \begin{bmatrix} x \\ y \\ 1 \end{bmatrix} = 0.$$

So, the quadratic form for the projection of a space sphere is:

$$C_S = \begin{bmatrix} (l^2-1)n_x^2 + (d_0+l \cdot n_z)^2 & (l^2-1)n_x n_y & (ld_0+n_z)f_e n_x \\ (l^2-1)n_x n_y & (l^2-1)n_y^2 + (d_0+l \cdot n_z)^2 & (ld_0+n_z)f_e n_y \\ (ld_0+n_z)f_e n_x & (ld_0+n_z)f_e n_y & f_e^2(d_0^2-n_z^2) \end{bmatrix}. \quad (9)$$

By setting  $d_0 = 0$  in (9), we obtain the quadratic form for the projection of a space line:

$$C_L = \begin{bmatrix} (l^2-1)n_x^2 + l^2 n_z^2 & (l^2-1)n_x n_y & f_e n_z n_x \\ (l^2-1)n_x n_y & (l^2-1)n_y^2 + l^2 n_z^2 & f_e n_z n_y \\ f_e n_z n_x & f_e n_z n_y & -f_e^2 n_z^2 \end{bmatrix}. \quad (10)$$

It is not difficult to prove that equation (10) is equivalent to the equation for a line image derived in [9], but our equation (10) has a more concise form. From equation (9) and (10), we notice that the metric catadioptric projections of a line and a sphere are both conics.

### 3.2. Invariants of line and sphere images

Under the metric catadioptric projection, if the projection of a sphere is  $C_S = \begin{bmatrix} a & b & d \\ b & c & e \\ d & e & f \end{bmatrix}$ , there exist two

invariants:

**Invariant 1.**  $S_1 = d(bd - ae) - e(be - cd) = 0$ .

**Invariant 2.**  $S_2 = b(bd - ae)f_e^2 - e(bf - de)(l^2 - 1) = 0$ .

Under the metric catadioptric projection, if the

projection of a line is  $C_L = \begin{bmatrix} a & b & d \\ b & c & e \\ d & e & f \end{bmatrix}$ , there exist three

invariants:

**Invariant 3.**  $L_1 = d(bd - ae) - e(be - cd) = 0$ .

**Invariant 4.**  $L_2 = bf + de(l^2 - 1) = 0$ .

**Invariant 5.**  $L_3 = d(bd - ae)f_e^2 + f(bf - de) = 0$ .

From  $n_x^2 + n_y^2 + n_z^2 = 1$  and formula (9) and formula (10), we can easily verify that Invariants 1~5 are true. The derivations of these invariants are given in [17]. The geometric interpretations of Invariant 1 and Invariant 3 are that one of major axes of the image conic passes through the origin of the image plane. This property had been discovered by many researchers [9] [10]. Invariant 5 can be derived from Invariant 4 and Invariant 2. Obviously, Invariants 1~5 do not contain variables  $n_x$ ,  $n_y$ ,  $n_z$  and  $d_0$ . That means these invariants do not change no matter where lines and spheres are located in the 3D space. The proof of the independency of Invariant 1 and 2 is omitted here, as well as that of Invariant 3, 4 and 5. These invariants will be used to derive the constraint equations for the intrinsic parameters in Section 3.4.

From above, we notice that, in general, a line image can provide three invariants (constraints), and a sphere

image can provide two. The reason is that, a general conic can provide five constraints, the orientation of the plane containing the great circle corresponding to the space line has two unknowns ( $n_x, n_y, n_z$ , with  $n_x^2 + n_y^2 + n_z^2 = 1$ ), and the plane containing the small circle corresponding to the space sphere has three unknowns ( $d_0$  and  $n_x, n_y, n_z$ , with  $n_x^2 + n_y^2 + n_z^2 = 1$ ). In the next section, we will discuss the invariants provided by the projections of lines and spheres in the degenerated cases.

### 3.3. Singularities of invariants

We describe here the singularities of invariants from the projections of lines and spheres. Due to lack of space, we are only able to give a sketch of the derivations. A first remark is that if and only if the metric catadioptric image conics of lines and spheres degenerate into lines or circles, there exist singularities. A second observation is that for these singular cases there exist necessary and sufficient conditions (see Proposition 1 and Proposition 2).

**Proposition 1.** *The metric catadioptric projection of a line (or a sphere) in space is a circle, if and only if  $l = 1$  or  $n_z = 1$ .*

**Proposition 2.** *The metric catadioptric projection of a line (or a sphere) in space is a line, if and only if the plane containing the corresponding great circle (or the corresponding small circle) passes through the optical center of the virtual camera.*

The proofs of Proposition 1 and Proposition 2 are omitted due to limited space. All singular cases derived from Proposition 1 and Proposition 2 are listed in Table 2. Note that the method in [8] deals with the paracatadioptric camera calibration using projections of lines in space is the singularity Case 1. In this case, one line image gives rise to three invariants, the two of them are:

$$a = c \quad b = 0. \quad (11)$$

Substituting  $b = 0$  and  $l = 1$  into Invariant 5, we obtain the third one:

$$f_e^2 = -\frac{f}{a}. \quad (12)$$

From formula (12), we can derive Proposition 1 in [8] which is the key proposition in that paper. The derivation is given in [17].

For Case 3 and 4, the centers of these image circles are all located at the origin of the image plane, then:

$$\begin{aligned} a &= c & b &= 0 \\ d &= 0 & e &= 0 \end{aligned} \quad (13)$$

For Case 3, we can get another invariant:

$$af_e^2 + fl^2 = 0. \quad (14)$$

The case where  $l=0$  and the projections of space spheres are used for calibration, is not a singular one since the projection of a sphere is a general conic in this case. A method for the conventional camera calibration using sphere images, proposed in [10], is a special case of our method, since it is well known that the catadioptric camera with a planar mirror is equivalent to a conventional camera. If we substitute  $l=0$  into Invariant 2, we obtain:

$$f_e = \sqrt{\frac{e(bf - de)}{b(ae - bd)}}. \quad (15)$$

It is not difficult to verify that formula (15) is equivalent to the formula of the effective focal length derived in [10].

Case	Conditions	Image	Invariants
1	$l=1$	PLS	(1), (2)
2		PSS	(1)
3	$n_z=1$	PLS	(3), (4)
4		PSS	(3)
5	$l=0$	PLS	-
6	$n_z=0$	PLS	-
7	$l \cdot n_z = d_0$	PSS	-

**Table 2:** Singularities of invariants from the projections of lines and spheres. Note that if the image conics degenerate into lines, the corresponding constraints (invariants) will vanish. "PLS" is the abbreviation for "Projection of Line in Space", and "PSS" for "Projection of Sphere in Space".

### 3.4. Constraints on the intrinsic parameters

In order to derive the constraint equations for the intrinsic parameters from the invariants derived before, we decompose the intrinsic matrix  $K$  defined in (2) into the product of two matrices:

$$K = K_A K_M, \quad (16)$$

where

$$K_A = \begin{bmatrix} r & s' & u_0 \\ & 1 & v_0 \\ & & 1 \end{bmatrix}$$

and  $s' = s/f_e$ . The matrix  $K_M$  is defined in (5).

Under the metric catadioptric projection, i.e., where the intrinsic matrix is equal to  $K_M$ , the equation of an image conic (a projection of a line or a sphere) derived in Section 3.1 can be rewritten as:

$$m^T A m = 0,$$

where

$$A = \begin{bmatrix} a & b & d \\ b & c & e \\ d & e & f \end{bmatrix}, \quad m = \begin{bmatrix} x \\ y \\ 1 \end{bmatrix}.$$

For the case of the generic catadioptric projection, i.e., the

intrinsic matrix  $K$  defined by (2), the equation of an image conic (a projection of a line or a sphere) is represented as:

$$m'^T A' m' = 0,$$

where

$$A' = \begin{bmatrix} a' & b' & d' \\ b' & c' & e' \\ d' & e' & f' \end{bmatrix}, \quad m' = \begin{bmatrix} u \\ v \\ 1 \end{bmatrix}.$$

$m'$  are the pixel coordinates in the image coordinate system. The image conic can be extracted from the actual catadioptric image using some conic fitting method, so the entries of matrix  $A'$  can be known prior to estimating the intrinsic parameters whereas the entries of matrix  $A$  still keep unknown. From the definitions of  $m$  and  $m'$ , we get:

$$m' = K_A m.$$

So,

$$A = K_A^T A' K_A$$

or

$$\begin{bmatrix} a & b & d \\ b & c & e \\ d & e & f \end{bmatrix} = \begin{bmatrix} r & s' & u_0 \\ & 1 & v_0 \\ & & 1 \end{bmatrix}^T \begin{bmatrix} a' & b' & d' \\ b' & c' & e' \\ d' & e' & f' \end{bmatrix} \begin{bmatrix} r & s' & u_0 \\ & 1 & v_0 \\ & & 1 \end{bmatrix}. \quad (17)$$

Expand the right side of (17), we can obtain:

$$\begin{cases} a = r^2 a' \\ b = r s' a' + r b' \\ c = s'^2 a' + 2 s' b' + c' \\ d = r u_0 a' + r v_0 b' + r d' \\ e = s' u_0 a' + u_0 b' + s' v_0 b' + v_0 c' + s' d' + e' \\ f = u_0^2 a' + 2 u_0 v_0 b' + v_0^2 c' + 2 u_0 d' + 2 v_0 e' + f' \end{cases}. \quad (18)$$

From the discussions in Section 3.2, we know that, in the nonsingular cases, the entries of matrix  $A$  must satisfy the invariants though these entries are yet unknown. Substituting (18) into Invariant 1 and 2, we obtain two constraint equations for the intrinsic parameters from an image conic of a space sphere. Similarly, substituting (18) into Invariant 3, 4 and 5, we obtain three constraint equations from an image conic of a space line. There are totally 6 unknown parameters to be calibrated: 5 intrinsic parameters and one parameter  $l$ . It is sufficient to estimate these parameters if there are 6 independent equations available. The six equations can be provided by either two line images or three sphere images.

For the singular cases presented in Section 3.3, we substitute (18) into the invariants provided by those image conics (see Table 2), then we can obtain the constraint equations for the intrinsic parameters in these cases. Here we only discuss how to obtain the constraint equations in the singular Case 1. Substituting (18) into (1), we obtain:

$$\begin{cases} r^2 a' = s'^2 a' + 2 s' b' + c' \\ r s' a' + r b' = 0 \end{cases}.$$

Solving for  $r, s'$ , we have:

$$\begin{cases} r = \sqrt{-\frac{b'^2}{a'^2} + \frac{c'}{a'}} \\ s' = -\frac{b'}{a'} \end{cases}$$

Substituting (18) into (12), we have:

$$\left(-\frac{b'^2}{a'} + c'\right)f_e^2 + a'u_0^2 + 2b'u_0v_0 + c'v_0^2 + 2d'u_0 + 2e'v_0 + f' = 0.$$

Since a line image can provide two constraint equations for  $r, s'$  and one constraint equation for  $u_0, v_0, f_e$ , at least three line images can perform calibration in Case 1.

Table 3 shows that the minimum number of line or sphere images should be used to achieve the calibration for different types of central catadioptric cameras. We assume these space lines and spheres are all in general position. Note that the minimum number of space lines for calibration have been discussed in [9] when the aspect ratio and the skew factor of the catadioptric camera are known in advance.

	Planar $l=0$	Hyperboloidal (Ellipsoidal) $0 < l < 1$	Paraboloidal $l=1$
PLS	-	2	3
PSS	3	3	*

**Table 3:** The minimum number of lines or spheres for the calibration of different types of central catadioptric cameras. The meanings of PLS and PSS are the same as those in Table 2.

\* In this case, we can only recover part of the intrinsic parameters (i.e.,  $r$  and  $s'$ ).

## 4. Calibration algorithm

In order to efficiently solve the nonlinear constraint equations of the intrinsic parameters, we present a two-stage calibration technique for the case where the number of line or sphere images is greater than or equal to four in the nonsingular cases.

### 4.1. Two-stage calibration technique

The theoretical basis of this technique is the following two observations.

**Observation 1:** The 6 constraint equations for the intrinsic parameters provided by two line images or three sphere images are non-linear. Generally speaking, it is quite hard to solve systems of non-linear equations.

**Observation 2:** The constraint equations for the intrinsic parameters derived from Invariant 1 or 3 are only for the parameters  $r, s', u_0$  and  $v_0$ , but not for  $l$  and  $f_e$ . If there are four or more sphere or line images, we have four or more constraint equations derived from Invariant 1 or 3.

Therefore we can use a non-linear least squares method to solve  $r, s', u_0$  and  $v_0$  provided good initial values of these parameters are available. Without loss of generality, we only describe here the two-stage algorithm based on sphere images, the two-stage algorithm using line images can be constructed in a similar way. The complete algorithm consists of the following stages:

**Stage 1:** Compute  $r, s', u_0$  and  $v_0$ .

Given four or more sphere images, derive the constraint equations from Invariant 1, and subsequently use Levenberg-Marquardt algorithm to recover  $r, s', u_0$  and  $v_0$  from these constraint equations. The initial estimations will be discussed in the next section.

**Stage 2:** Compute  $l$  and  $f_e$ .

Substituting the results  $r, s', u_0$  and  $v_0$  obtained in the first stage into (17), and then substituting the entries of matrix  $A$  obtained from (17) into Invariant 2, we get a quadric equation for the parameters  $l$  and  $f_e$ . Therefore, in this stage, two sphere images are sufficient to solve  $l$  and  $f_e$  using the intersections of the two quadric curves. For a catadioptric camera, the parameter  $l$  usually keeps constant. If  $l$  is known in advance, one sphere image is sufficient to solve the parameter  $f_e$ .

Since the initial guesses of parameters  $l$  and  $f_e$  are not necessary, we only need to find the initial values of  $r, s', u_0$  and  $v_0$  as shown in the next section.

### 4.2. Initial estimations

Similar to [5], the method for finding initial values is to identify the bounding ellipse of the catadioptric image. This can be done by using a predefined threshold, finding the boundary, and fitting an ellipse to the resulting boundary. Note that the boundary is the projection of the mirror boundary which is a circle. The plane containing the circle is perpendicular to the optical axis of the camera and the optical axis goes through the center of the circle. It is not difficult to prove that this case is equivalent to the singular Case 4. From Table 2, we know that the image of the boundary can provide four constraints as shown in (13). Substituting (18) into (13), and after some manipulation, the initial values of  $r, s', u_0$  and  $v_0$  can be obtained:

$$\begin{cases} r = \sqrt{-\frac{b'^2}{a'^2} + \frac{c'}{a'}} \\ s' = -\frac{b'}{a'} \\ u_0 = \frac{b'e' - c'd'}{a'c' - b'^2} \\ v_0 = \frac{b'd' - a'e'}{a'c' - b'^2} \end{cases}$$

where the initial values of  $(u_0, v_0)$  is the center of the bounding ellipse.

## 5. Experiments

We have performed a number of experiments with simulated and real data, in order to assess the performances of our calibration algorithm. We use a perspective camera with a hyperbolic mirror, designed by the Center for Machine Perception, Czech Technical University, its field of view is about 210 degree, and the eccentricity of the hyperbolic mirror is  $\varepsilon=1.3017$ . From formula (4), we get  $l=0.9662$ . In these experiments, we assume that the parameter  $l$  is known in advance.

### 5.1. Simulations

The simulated camera has the following parameters:  $r=1$ ,  $s=0$ ,  $u_0=750$ ,  $v_0=600$  and  $f_e=400$ . The resolution of the image is  $1500 \times 1200$ . We generate two different images: the first one contains the projections of 5 space lines and the second one contains the projections of 5 space spheres. The variables  $n_x$ ,  $n_y$ ,  $n_z$  and  $d_0$  which are used to represent the 3D locations of these lines and spheres are uniformly distributed within their valid ranges. The projection of the mirror boundary is also generated in each image. Since it is difficult to select a good fixed threshold due to lighting changing and nonuniformity of directional lighting, we only select about one-third of the entire ellipse of the boundary to simulate the actual conditions. On each projection curve we choose about 50 points. Gaussian noise with zero-mean and  $\sigma$  standard deviation is added to these image points. We vary the noise level  $\sigma$  from 0.1 to 2.0 pixels. The simulated images are shown in Figure 2. The conic fitting algorithms used here are those presented in [15] and [16]. For each noise level, we perform 100 independent trials, and the mean values of these recovered parameters are computed as the estimations over each run. The calibration results for 5 sphere and 5 line images using our two-stage method are shown in Table 4a and Table 4b, respectively. The calibration results using the method presented in [6] are shown in Table 4c for comparison purposes. In Table 4, the skew factor  $s$  is replaced by  $\theta$  which is the angle between the two image coordinate axes. The relative error of the aspect ratio is  $|r-r^*|/r$  where  $r$  is the ground truth and  $r^*$  is the mean, and the relative errors of other parameters are defined in the same way. The results show that, the method using sphere images is more robust and more accurate than the method based on line images. The main reason for this may be attributed to the fitting accuracy of

sphere images higher than that of line images (see Figure 2).

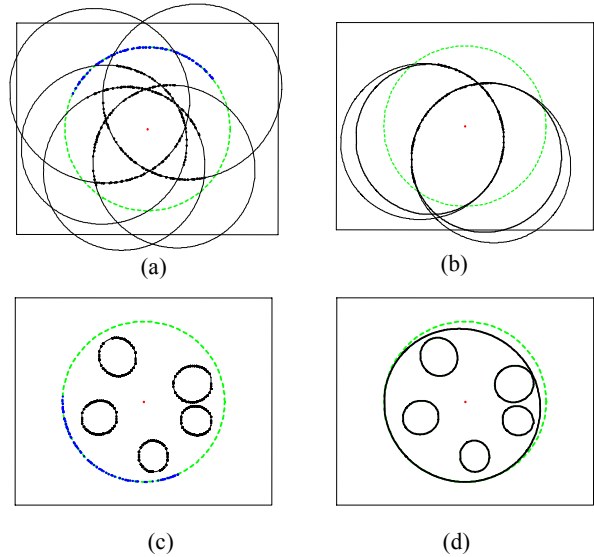


**Figure 2:** (a) and (c) are simulated images containing the projections of five lines and five spheres, respectively. (b) and (d) are the images after conic fitting from (a) and (c) when Gaussian noise of standard deviation 2.0 pixels is added. For the convenience of visualization, only two fitted conics are shown in (b). The ground truths of the projections are shown by the thin solid line, and the fitted conics are shown by the thick solid line. More explicitly, the fitting results of sphere images are better than those of line images.

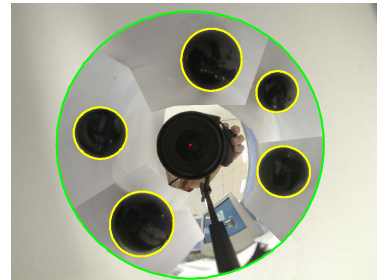


**Figure 3:** A real image in our experiments. The resolution of the image is  $2048 \times 1536$ . The conic fitting results are shown in this image.

### 5.2. Real data

The test spheres for the real image experiments are billiard balls. These balls are placed in front of a white screen in order to create high contrast lighting environments. We take images of these balls using the catadioptric camera described before. Image conic extracting is accomplished by a software package developed by our group. One of the experimental images is shown in Figure 3. The calibration results with real data

are listed in Table 5.

(a): Using our method from sphere images					
Noise level	$r$ (%)	$\theta$ (%)	$u_0$ (%)	$v_0$ (%)	$f_e$ (%)
0.4	0.022	0.001	0.369	0.239	0.173
0.8	0.028	0.002	0.431	0.252	0.386
1.2	0.033	0.006	0.404	0.314	0.940
1.6	0.032	0.010	0.907	0.363	1.814
2.0	0.040	0.013	1.069	0.476	2.648

(b): Using our method from line images					
Noise level	$r$ (%)	$\theta$ (%)	$u_0$ (%)	$v_0$ (%)	$f_e$ (%)
0.4	0.115	0.021	4.990	2.468	4.579
0.8	0.846	0.026	8.503	2.539	9.837
1.2	1.505	0.032	11.875	4.465	14.439
1.6	2.571	0.031	13.217	8.522	18.863
2.0	2.543	0.034	14.004	9.122	20.169

(c): Using the method in [6] from line images					
Noise level	$r$ (%)	$\theta$ (%)	$u_0$ (%)	$v_0$ (%)	$f_e$ (%)
0.4	0.902	0.162	1.192	0.499	1.966
0.8	0.396	0.379	4.635	1.395	7.552
1.2	0.791	0.549	9.212	2.875	15.798
1.6	1.249	0.845	15.097	6.871	29.162
2.0	1.674	1.309	22.346	6.957	49.188

**Table 4:** The relative errors while using different calibration methods

	Initial estimations	Final results
$r$	1.0017	$1.0035 \pm 0.0006$
$s'$	0.0137	$-5.87 \times 10^{-4} \pm 5.4 \times 10^{-5}$
$u_0$	997.1	$993.2 \pm 3.4$
$v_0$	784.3	$787.8 \pm 2.7$
$f_e$	-	$503.8 \pm 4.9$

**Table 5:** Calibration results with real data

## 6. Conclusion

In this paper, we present a unified framework for the calibration of central catadioptric cameras based on images of lines or spheres in space. The constraint equations for the intrinsic parameters given by the projection of a space line as well as by the projection of a space sphere are derived. The minimum number of line or sphere images for the calibration of different types of central catadioptric cameras is clarified in this paper. In order to efficiently solve the non-linear equations of the intrinsic parameters, we present a two-stage calibration technique which divides the intrinsic parameters into two groups and uses the Levenberg-Marquardt algorithm to perform the minimization to estimate the intrinsic parameters. The experimental results show that the

calibration method based on sphere images is more robust and has higher accuracy than that using line images.

## References

- [1] S. Baker and S.K. Nayar, "A Theory of Catadioptric Image Formation", *In Proc. International Conference on Computer Vision*, India, 1998, pp. 35-42.
- [2] S.A. Nene and S.K. Nayar, "Stereo with mirrors", *In Proc. International Conference on Computer Vision*, India, 1998, pp. 1087-1094.
- [3] T. Svoboda, T. Padjla, and V. Hlavac, "Epipolar geometry for panoramic cameras", *In Proc. European Conference on Computer Vision*, 1998, pp. 218-231.
- [4] D.G. Aliaga, "Accurate Catadioptric Calibration for Real-time Pose Estimation of Room-size Environments", *In Proc. International Conference on Computer Vision*, Canada, 2001, pp. 127-134.
- [5] S.B. Kang, "Catadioptric self-calibration", *In IEEE Conference on Computer Vision and Pattern Recognition*, 2000, pp. 201-207.
- [6] J.P. Barreto and H. Araújo, "Geometric Properties of Central Catadioptric Line Images", *In Proc. European Conference on Computer Vision*, 2002, pp. 237-251.
- [7] C. Geyer and K. Daniilidis, "Catadioptric camera calibration", *In Proc. International Conference on Computer Vision*, 1999, pp. 398-404.
- [8] C. Geyer and K. Daniilidis, "Paracatadioptric Camera Calibration", *IEEE Transactions on Pattern Analysis and Machine Intelligence*, 2002, 24(5): pp. 687-695.
- [9] C. Geyer and K. Daniilidis, "A Unifying Theory for Central Panoramic Systems and Practical Implications," *In Proc. European Conference on Computer Vision*, 2000, pp. 445-462.
- [10] N. Daucher, M. Dhome, and J-T Lapresté, "Camera Calibration From Spheres Images", *In Proc. European Conference on Computer Vision*, 1994, pp. 449-454.
- [11] S. Bogner, "Introduction to Panoramic Imaging", *in Proc. IEEE International Conference on Systems Man and Cybernetics*, Vancouver, 1995, pp. 3100-3106.
- [12] Y. Yagi and S. Kawato, "Panorama scene analysis with conic projection," *in Proc. IEEE International Workshop on Intelligent Robots and Systems*, 1990, pp. 181-187.
- [13] J. Hong, X. Tan, R. Weiss, and E. Riseman, "Image-based homing", *In IEEE International Conference on Robotics and Automation*, 1991, pp. 620-625.
- [14] V. Nalwa, "A true Omnidirectional Viewer", Technical report, Bell Laboratories, Holmdel, U.S.A., February 1996.
- [15] Z. Zhang, "Parameter Estimation Techniques: A Tutorial with Application to Conic Fitting", INRIA Rapport de Recherche n 2676, October 1995.
- [16] A. Fitzgibbon, M. Pilu, and R. Fisher, "Direct least-square fitting of ellipses", *In Proc. International Conference on Pattern Recognition*, 1996, pp. 253-257.
- [17] X. Ying and Z. Hu, "Catadioptric Camera Calibration Using Geometric Invariants", Technical Report, National Laboratory of Pattern Recognition, CAS, December 2002.